# 8B.7 INTELLIGENT MITIGATION OF NORMAL AND ANOMALOUS PROPAGATION CLUTTER

M. Dixon, J.C. Hubbert*, S. Ellis, C. Kessinger and G. Meymaris
National Center for Atmospheric Research, Boulder CO

## 1. INTRODUCTION

Echoes from normal propagation ground clutter (NP) as well as anomalous propagation ground clutter (AP) contaminate weather echoes so that precipitation estimates based on such contaminated echoes are biased. The problem is typically mitigated by applying a clutter filter to all radar data but this also eliminates weather data at zero velocity. With the advent of fast digital receivers, the real time identification and filtering of clutter is now possible. To do this, fuzzy logic is used to distinguish between clutter echoes and precipitation echoes. Based on this classification, clutter filters can be applied to only those radar resolution volumes where clutter is present, in real time. In this way weather echoes are preserved while clutter echoes are mitigated. The clutter filters used in this paper are spectral based, i.e., they are applied in the spectral domain. In many cases, after the clutter echoes are filtered, the underlying weather echo signatures are revealed thereby significantly increasing the visibility of weather echo. This paper describes the Fuzzy Logic algorithm for clutter echo identification and the technique is illustrated with experimental data from the Denver NEXRAD KFTG and S-Pol, NCAR's (National Center for Atmospheric Research) S-band polarimetric radar.

## 2. BACKGROUND

Clutter filters for weather radars typically operate in the time domain, i.e., the digitized I and Q samples (in-phase and quadrature) are passed through some type of IIR (Infinite Impulse Response) filter. These filters work fairly well typically yielding 50 dB of clutter rejection or better. Different stop-band filter widths are possible but the clutter filter is typically applied to all of the radar data, i.e, the clutter filters are either on or off all the time. If the clutter filters are on all the time, weather signals along the zero velocity isodop are also removed. Additionally, as weather conditions vary, AP clutter can appear and subsequently disappear. To avoid necessary clutter filter usage, radar operators have attempted to monitor AP clutter and then turn on a clutter filter when the AP conditions were significant. Later the clutter filter is turned off. Such human-driven decisions are prone to error. Ideally the clutter filter is applied only to radar gates that are clutter-contaminated and only when the clutter power can affect the radar signatures due to an overlaying weather signal. Applying a clutter filter to those gates that lie on a previously constructed map of NP (Normal Propagation) clutter can eliminate important weather signals. For example, there may be a radar gate that shows 35 dBZ on a clutter map that is overlaid with a 45 dBZ or greater weather signal. In this case, a clutter filter likely should not be applied, particularly if the weather velocity is close to zero. The solution is to use signal processing to identify those gates that are dominated by clutter and then to apply a clutter filter to those gates in real time.

### *2.1 Spectral Clutter Filters*

The new generation of radar processors now have enough processing power to calculate spectra, process them, and subsequently apply a clutter filter if needed. The I and Q samples can be put into a buffer while the data is processed and clutter-affected gates are identified. After identification, the buffered data is filtered. The additional processing power also allows for cluttering filtering in the "frequency" or velocity domain, i.e., the I and Q samples are Fourier transformed via an FFT algorithm after which the signal spectrum can be processed. The new spectral clutter filters not only remove power around zero velocity in the spectra but also use an interpolation scheme to fill in the spectral points that were "notched" out (i.e., set to zero) (Siggia and Passarelli 2004). Such filters can first adaptively set a filter notch width according to the characteristics of the spectrum, and then fit a Gaussian shaped curve to the remaining assumed weather signal. The fitted Gaussian curve is used to interpolate across the notch left in the spectrum due

*NCAR/EOL, Boulder, Colorado 80307, email: hubbert@ucar.edu

to the clutter filter. Figures 1 and 2 illustrate this process. Shown in Fig. 1 are a weather spectrum (red), a clutter signal spectrum (green) and the combination of these two spectra (blue). Fig. 2 shows the same spectra but with the Gaussian-fitted curve in red dots and the resultant clutter filtered spectrum in black. If the interpolated area (around zero velocity) were replaced with a notch (set to zero), an obvious bias in both power and velocity estimates of the weather echo would occur. Such an adaptive spectral based clutter filter is used in this paper.

## 3. FUZZY LOGIC IDENTIFICATION

To identify the gates that are contaminated with clutter, a Fuzzy Logic based algorithm termed CMD (Clutter Mitigation Decision) is employed. First it is noted that narrow spectrum width, zero velocity weather echoes (such as from stratiform rain) are very difficult to distinguish from clutter based solely on their spectra and thus spatial textures of various radar measureables are used in order to make this distinction.

### 3.1 *Single Polarization Algorithm*

To identify clutter echoes and distinguish them from narrow spectrum width, zero velocity weather echoes, three variables, or feature fields, are used in the single polarization case: 1) spatial texture of reflectivity, 2) the so-called SPIN of reflectivity (Steiner and Smith 2002) and 3) the Clutter Phase Alignment (CPA). The texture of the reflectivity (TDBZ) is computed as the mean of the squared reflectivity difference between adjacent gates,

$$TDBZ = \left[ \sum_{j}^{L} \sum_{i}^{M} (dBZ_{i,j} - dBZ_{i-1,j})^2 \right] /N \quad (1)$$

where dBZ is the reflectivity, L is the number of radar beams or rays used, M is the number gates used and $N = L * M$. In this paper, L is equal to one, i.e., only data along a single radar radial is used to calculate TDBZ (and SPIN), which eliminates the need to buffer adjacent beam information into memory and significantly reduces the algorithm complexity over the use of 2-D computations. The TDBZ feature field is computed at each gate along the radial with the computation centered on the gate of interest. The SPIN feature field is a measure of how often the reflectivity gradient changes sign along a direction in space (in this case the radar radial) (Steiner and Smith 2002).

### 3.2 *Clutter Phase Alignment*

The Clutter Phase Alignment (CPA) is calculated from a length N time series $x_i$ as

$$CPA = \left| \sum_{i=1}^{N} x_i \right| / \left[ \sum_{i=1}^{N} |x_i| \right] \quad (2)$$

If the $\arg\{x_i\}$ is the same for all $x_i$ then $CPA = 1$. Thus, CPA is the magnitude of the vector sum of the individual time series members divided by the the sum of the magnitudes of the $x_i$. CPA is an excellent indicator/identifier of clutter since by definition it is a measure of the primary characteristic of a stationary ground clutter target, i.e., constant backscatter phase. In fact, if the phase of the $x_i$ is a constant, CPA will be one regardless of the behavior of the magnitude of the $x_i$. CPA is a measure of how constant the absolute return phase (i.e., the phase of a received I and Q sample) is for a resolution volume. For a fixed, non moving target, CPA is 1. If the target is not completely stationary over the measurement period, the mean velocity will differ from 0 ms$^{-1}$ and/or the width of the spectrum of the radar return signal will increase. Both nonzero mean velocity and increased spectrum width will decrease CPA to below 1. The more constant the absolute phase is, the more likely it is that the gate contains clutter. For pure clutter, CPA is usually greater than 0.95 while it is about zero for noise and weather with mean velocity magnitude greater than 1 ms$^{-1}$ (ignoring the possibility of velocities that "wrap" back to 0 ms$^{-1}$). Only weather echoes with velocity magnitude $<$ 0.3ms$^{-1}$ (approximately) and spectrum widths less than about 0.5 ms$^{-1}$ have CPA values close to 0.95. Thus, the reflectivity texture and SPIN fields are needed to distinguish these echoes from clutter. In any event, CPA is nearly always significantly less than 0.95 for weather time series that are collected over times that are significantly longer than the decorrelation time of the precipitation particles in the radar resolution volume.

There is a close relationship between CPA and the velocity and spectrum width. Figure 3 show this relationship. Time series simulations were made for velocities from -0.6 ms$^{-1}$ to 0.6 ms$^{-1}$ at 0.1 ms$^{-1}$ steps, 100 simulations per step. The simulation parameters are: PRT=1ms, $\sigma_v = 0.1$ ms$^{-1}$, 64 points,and SNR=60 dB. For each simulated time series the velocity is estimated via the pulse pair algorithm, CPA is calculated and the result is shown in Figure 3. As can be seen, as velocity magnitude increases, the value of CPA decreases rather quickly. When the velocity magnitude is greater than $0.2\,\mathrm{ms}^{-1}$, the average CPA values are below 0.9. Both velocity and spectrum affect CPA: 1) as the velocity departs from zero, CPA decreases rapidly, 2) as the spectrum width increases the value of CPA decreases. There are well known variances associated with the pulse pair velocity estimator and especially the width estimator, furthermore, no particular spectrum shape is assumed for the CPA calculation as is done with the pulse pair estimators. Thus, CPA is a more robust indicator of clutter than radial velocity and spectrum width.

There is another interesting relationship between CPA and the spectrum of the signal. The numerator of CPA is identical to the 0 velocity component of the discrete Fourier transform (DFT) the signal (within a scale factor N). Thus, it is natural to compare CPA to the ratio of the 0 velocity component of the DFT to the total power of the signal. This is referred to as the Power Ratio (PR). First, let $x_i$ be a time series sequence and let $X_m$ be the DFT of $x_i$. Parseval's relationship for the DFT states

$$\sum_i |x_i|^2 = \frac{1}{N}\sum_m |X_m|^2. \tag{3}$$

The inequality we hypothesize is

$$\begin{aligned} CPA \quad &\geq \quad \sqrt{(PR)} && (4)\\ \frac{|\sum_{i=1}^{N} x_i|}{\left[\sum_{i=1}^{N}|x_i|\right]} \quad &\geq \quad \sqrt{\frac{|X_0|^2}{\sum_m |X_m|^2}} && (5)\end{aligned}$$

The right hand side is rewritten in terms of $x_i$ as (using Parseval)

$$\frac{|\sum_{i=1}^{N} x_i|}{\left[\sum_{i=1}^{N}|x_i|\right]} \geq \sqrt{\frac{|\sum_{i=1}^{N} x_i|^2}{N\sum_{i=1}^{N}|x_i|^2}} \tag{6}$$

The numerators are equal and the inequality can be rewritten as

$$\left[\sum_{i=1}^{N}|x_i|\right] \leq \sqrt{N\sum_{i=1}^{N}|x_i|^2} \tag{7}$$

Dividing both sides by N gives

$$\frac{\left[\sum_{i=1}^{N}|x_i|\right]}{N} \leq \sqrt{\frac{\sum_{i=1}^{N}|x_i|^2}{N}} \tag{8}$$

This simply states that the root mean square average is greater than the arithmetic mean, a well known result. Thus we have proven the inequality of Eq. (5). The result indicates that CPA should be a better discriminator of clutter than the PR. To illustrate this, examine Fig. 4 which shows a scatter plot of CPA versus $PR^{0.5}$ for a low level PPI scan that contains both clutter and weather echoes collected by S-Pol. As can be seen, there exist many resolution volumes where the $PR^{0.5}$ is in the 0.5 to 0.7 range while CPA is close to one. Figures 5 and 6 show the times series of $I^2 + Q^2$ dBm and $\tan^{-1}(Q/I)$ degrees for a resolution volume with clutter where CPA=0.96 but $PR^{0.5} = 0.59$ (time series length 64). As can be seen the clutter target only becomes visible to the scanning radar about half-way through the collected time series. At this point the phase becomes fairly stable at around $-135°$. The difference between CPA and $PR^{0.5}$ can be explained as follows. Since the ground clutter target is only visible through about half of the I and Q samples, the power time series varies dramatically from -85 dBm to -55 dBm during which the phase remains fairly constant. This sharp gradient in the power time series spreads power away from the zero velocity component in the spectrum of the signal thereby reducing the the power ratio $PR^{0.5}$. This characteristic makes CPA a better discriminator of clutter for such scanned ground clutter targets.

### 3.2 *Fuzzy Logic Algorithm*

The Fuzzy Logic membership functions used in CMD are shown in Fig. 7. The membership functions are applied to TDBZ, SPIN and CPA resulting in so-called interest fields varying from 0 to 1 with 1 indicating the strongest clutter signal for the given variable. The TDBZ and SPIN interest field are then combined with a fuzzy "or" rule: the maximum interest value of TDBZ and SPIN is selected. The two remaining interest fields, MAX(TDBZ,SPIN) and CPA are multiplied by a-priori weights of 1.0 and 1.01 respectively and normalized by the sum of the weights. The weighted sum of interest values yields a probability of clutter between 0 and 1. Finally gates with values greater than 0.5 probability are classified as clutter. The chosen weight of 1.01 for CPA can be justified as follows. For certain cases MAX(TDBZ,SPIN) is zero while the CPA interest is one. In this case the normalized weighted sum (or probability) would be 0.5 if both interest fields had weights of one, and the point would be classified as not clutter. By giving CPA a weight of 1.01, such cases are classified as clutter. Through experience, this has proven to improve the performance of the CMD algorithm.

The general steps of the CMD algorithm are as follows:

1. Check if SNR $> 3$ dB, otherwise no filtering applied at this gate.
2. Compute feature fields texture of dBZ (TDBZ), dBZ SPIN and clutter phase alignment (CPA). The kernel for TDBZ computation is 1 beam by 9 range gates and for SPIN is 1 beam by 11 range gates.
3. Apply interest mapping to convert feature fields to interest values.
4. Compute CMD field by applying Fuzzy Logic to interest fields.
5. Combine TDBZ and SPIN interest fields using fuzzy or rule (maximum interest).
6. Compute normalized weighted sum of interest values.
7. Threshold CMD at 0.5 to produce CMD clutter flag.
8. Apply clutter filter where CMD flag is set.

### 3.3 *Dual polarization Fuzzy Logic*

The above clutter mitigation algorithm was designed for use with single polarization data; however, provision was also made for the inclusion of dual polarization parameters. The dual polarization inputs can be either "activated" or "deactivated" depending on the type of data processed. It was found that the spatial texture of copolar differential reflectivity ($Z_{dr}$) and copolar differential phase ($\phi_{dp}$) are excellent discriminators of clutter and weather. In our tests we found that kernels of 7 to 11 gates of data along a radial produced good discrimination between weather and clutter echoes, depending on the parameter. It was also found that the copolar correlation coefficient, $\rho_{hv}$, was not as good a discriminator as the textures of $Z_{dr}$ and $\phi_{dp}$ and therefore is not included in the Fuzzy Logic algorithm. The parameters used in the dual polarization CMD algorithm are summarized in Table 1 while the membership functions and the weights are summarized in Table 2. The membership functions for $\sigma_{zdr}$ and $\sigma_{\phi_{dp}}$ are given in Fig. 8.

## 4. EXPERIMENTAL DATA

### 4.1 *Single polarization data*

The following one half degree elevation angle PPI data were gathered with KFTG on 26 October 2006 in a wide-spread snow storm along the Eastern Foothills of the Rocky Mountains in Colorado. The times series data were gathered and the CMD algorithm was run during post processing. (However, the algorithm is designed to run in real time and currently does so on S-Pol.) Figs. 9 and 10 show unfiltered reflectivity and velocity, respectively. The x- and y-axes span 250 km and the range rings are in 30 km increments. The Rocky Mountains are easily seen in the left portion of the PPIs. Peak reflectivities are about 40 dBZ in the storm (wet snow) while the reflectivity due to the mountain clutter is in excess of 65 dBZ. The velocity plot shows a clear 0 velocity isodop through the center of the plot (in gray). The reflectivity shows areas marked by black lines that indicate the location of the zero velocity isodop. The velocity field shows areas where the velocity has folded back to $0\,\mathrm{ms}^{-1}$ (again in gray). The power in these areas will be severely attenuated if a clutter filter is applied. It is these 0 velocity weather areas that the CMD should *not* identify as clutter. Fig. 11 is a $0.5°$ clear air PPI scan and thus is a clutter map for the region displayed in Figs. 9 and 10. It is shown for reference. Fig. 12 shows the resulting reflectivity when a clutter filter is simply applied everywhere. Note that the reflectivity has been eliminated not only along the 0 velocity isodop but also in the areas of 0 velocity folded echoes as indicated in Fig. 10. Figure 12 is actual Archive 2 (A2) data downloaded from the NWS archive site: i.e., this is the data that was actually viewed by NWS forecasters and used by algorithms including the precipitation accumulation. Large errors are apparent due to the clutter filters being applied everywhere. This shows the problem when clutter filters are applied everywhere.

The CMD algorithm was used to create the clutter map shown in Fig. 13 with yellow marking the regions to be clutter filtered and this can be compared to Fig. 11. A spectral based clutter filter is now applied to the data at the gates indicated by Fig. 13 and the resulting reflectivity PPI is shown in Fig. 14. This should be compared to Fig. 9. The CMD clutter filtered reflectivity demonstrates the enormous improvement in data quality when compared to the actual A2 data of Fig. 12.

### 4.2 *Performance Evaluation*

To evaluate the performance of the CMD algorithm in identifying clutter, the SNR (signal-to-clutter ratio) is calculated for each gate. The clutter power is estimated as the power removed by the clutter filter. The remaining power is considered to be weather power. Gates with near zero velocity (i.e., $|vel| \leq 2\text{ms}^{-1}$) are excluded. The fraction of range gates CMD identifies for filtering as a function of the clutter to signal ratio (CSR) is determined. The results are shown in Fig. 15. The red line indicates the fraction of gates that were unfiltered whereas the blue line indicates the fraction of gates where the clutter filter was applied. One minus the blue line value gives the red line value. As can be seen the crossover point is located at about -8 dB CSR, that is about 50% of the gates with with CSR= -8 dB are clutter filtered. Since clutter with CSR of -10 dB can bias weather velocity estimates by 2 to $3\,\text{ms}^{-1}$ (depending on the true velocity of the weather) being able to identify weather contaminated by clutter with CSR down to -10 dB is a desirable goal. Ideally the crossover point would be at a CSR less than -10 dB but identifying clutter at such low CSR is difficult: the weather echoes dominate the calculated feature fields. Nevertheless, the CMD performance is excellent especially when considered against the alternative of applying the clutter filter everywhere.

### 4.2 *Dual Polarization Data*

The following data was gathered by S-Pol on 24 April 2007 in dual polarization mode. Figure 16 shows non-clutter filtered reflectivity while Fig. 17 shows non-clutter filtered velocity. Figure 18 shows clear air reflectivity and thus provides a NP clutter map for reference. To illustrate the discrimination capability of each of the Fuzzy Logic input variables, Figs. 19, 20, 21 and 22 show the interest fields of CPA, $\sigma_{zdr}$, $\sigma_{\phi_{dp}}$ and maximum(TDBZ, SPIN), respectively. All interests fields are very good clutter indicators with some being better than others in particular regions. Taken together, the interest fields provide a robust indicator of clutter.

Figure 23 shows the clutter map created by the dual polarization CMD algorithm. Clutter filters are then applied to the region designated in Fig. 23 and the resulting clutter filtered reflectivity is shown in Fig. 24. As can be seen the clutter is nicely mitigated leaving the meteorological echoes intact.

## 5. CONCLUSIONS

The Fuzzy Logic based Clutter Mitigation Decision (CMD) algorithm can effectively identify clutter in radar data. If a high speed processor is used, the CMD identified clutter contaminated data can be clutter filtered in real time. After the clutter filter has been applied to the data the radar moments can then be recalculated so that any remaining weather data may be revealed. The CMD algorithm used here employs a new feature field called Clutter Phase Alignment (CPA) which is an excellent discriminator of clutter. CMD has been designed to work with both both single as well as dual polarization data.

**Acknowledgment** This research was supported by the ROC (Radar Operations Center) of Norman OK. The National Center for Atmospheric Research is sponsored by the National Science Foundation. Any opinions, findings and conclusions or recommendations expressed in this publication are those of the author(s) and do not necessarily reflect the views of the National Science Foundation.

**References**

Dixon, M., C. Kessinger, and J.C. Hubbert, 2006: Echo classification within the spectral domain to discriminate ground clutter from meteorological targets. $86^{th}$ AMS Annual Meeting, IIPS, Atlanta, GA.

Siggia, A. and R. Passarelli, 2004: Gaussian model adaptive processing (GMAP) for improved ground clutter cancellation and moment calculation. Pro. of Third Euro. Conf. on Radar in Meteo. and Hydro (ERAD 2004). 67–73, Visby, Gotland, Sweden.

Steiner, M. and J.A. Smith, 2002: Use of three-dimensional reflectivity structure for automated detection and removal of non-precipitating echoes in radar data. *JTECH*, 9(5):673-686.

| Name | Type | Value | Description |
|---|---|---|---|
| NGATES_KERNEL_TDBZ | integer | 9 | Number of gates in kernel for TDBZ |
| NGATES_KERNEL_SPIN | integer | 11 | Number of gates in kernel for SPIN |
| NGATES_KERNEL_$\sigma_{zdr}$ | integer | 7 | Number of gates in kernel for $\sigma_{zdr}$ |
| NGATES_KERNEL_$\sigma_{\phi_{dp}}$ | integer | 7 | Number of gates in kernel for $\sigma_{\phi_{dp}}$ |
| SPIN_THRESHOLD | floating point | 5.0 | dBZ difference threshold used in SPIN calculation |
| SNR_THRESHOLD | floating point | 3.0 | Signal-to-noise ratio threshold for censoring total power, in dB |
| PROB_THRESHOLD | floating point | 0.5 | If the clutter probability exceeds this threshold the clutter flag is set |

Table 1: Description of the dual polarization CMD parameters.

| Field | Weights | Membership function break points |
|---|---|---|
| TDBZ | N.A. | (20, 0), (40,1) |
| SPIN | N.A. | (10, 0), (25,1) |
| MAX_TDBZ_SPIN | 1.0 | N.A. |
| CPA | 1.01 | (0.6, 1), (0.9, 1) |
| $\sigma_{zdr}$ | 0.5 | (1.2, 1), (2.4, 1) |
| $\sigma_{\phi_{dp}}$ | 0.5 | (10, 1), (15, 1) |

Table 2: Description of the dual polarization CMD parameters.

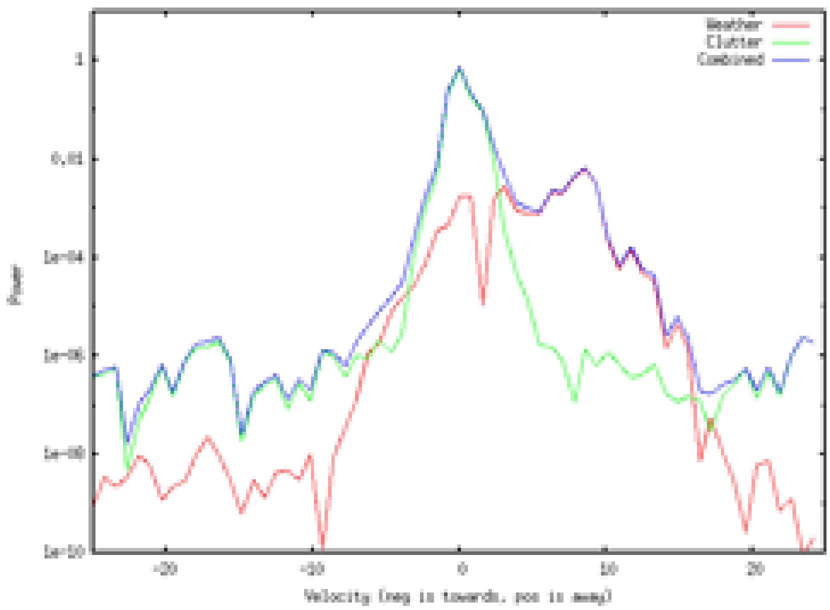


Figure 1: Example of weather and clutter spectra.

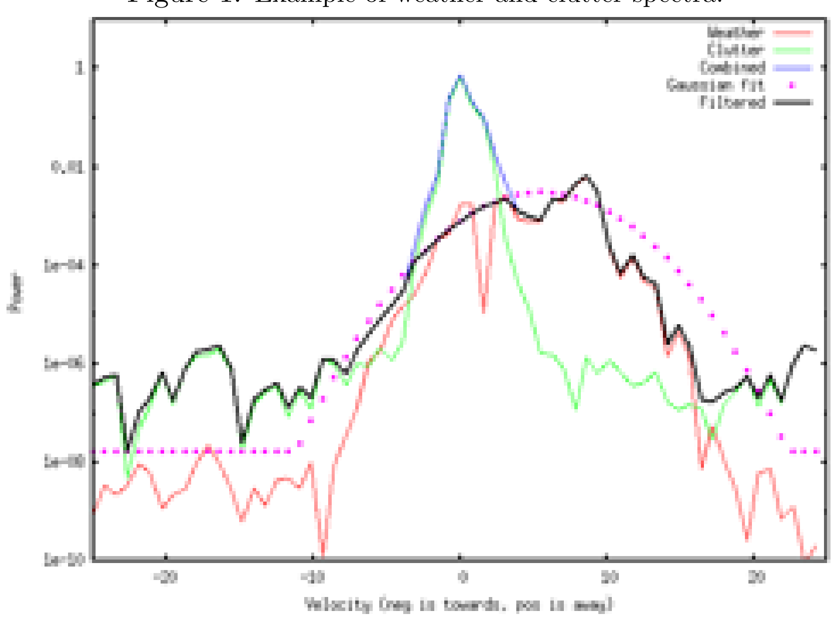


Figure 2: Example of spectral filter.

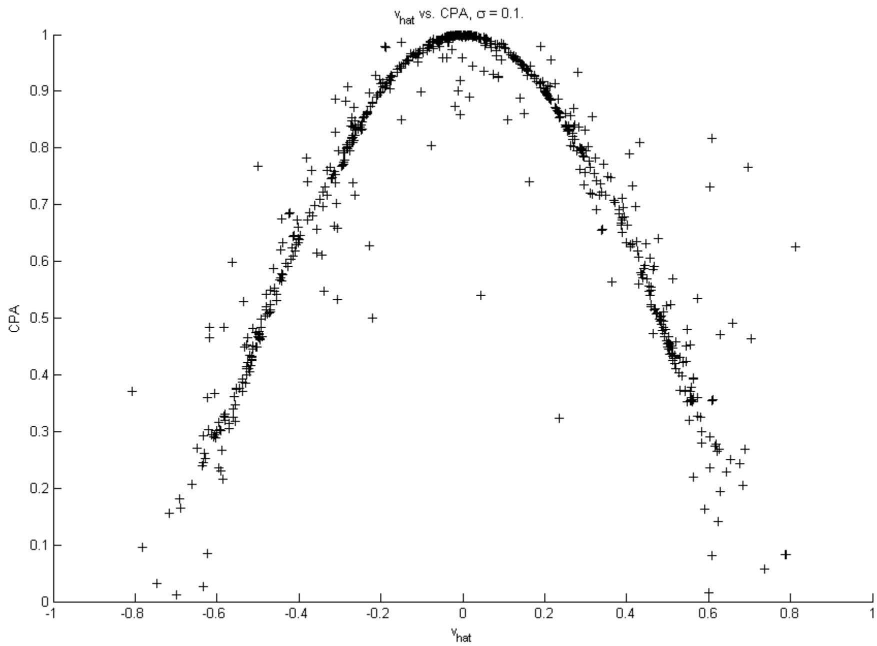


Figure 3: *Scatter plot of CPA versus Doppler velocity for simulated data*

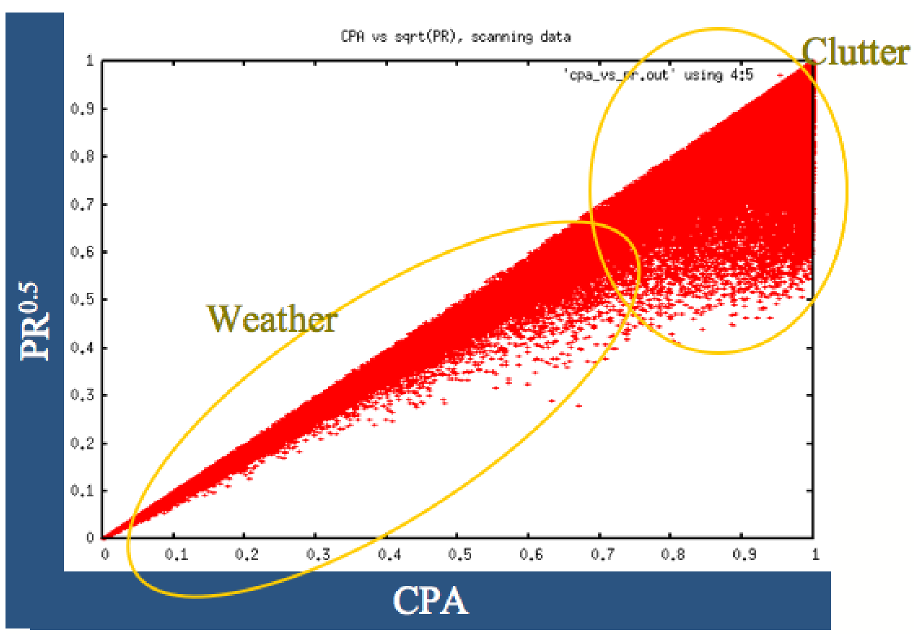


Figure 4: *Scatter plot of CPA versus $PR^{0.5}$ for experimental data*

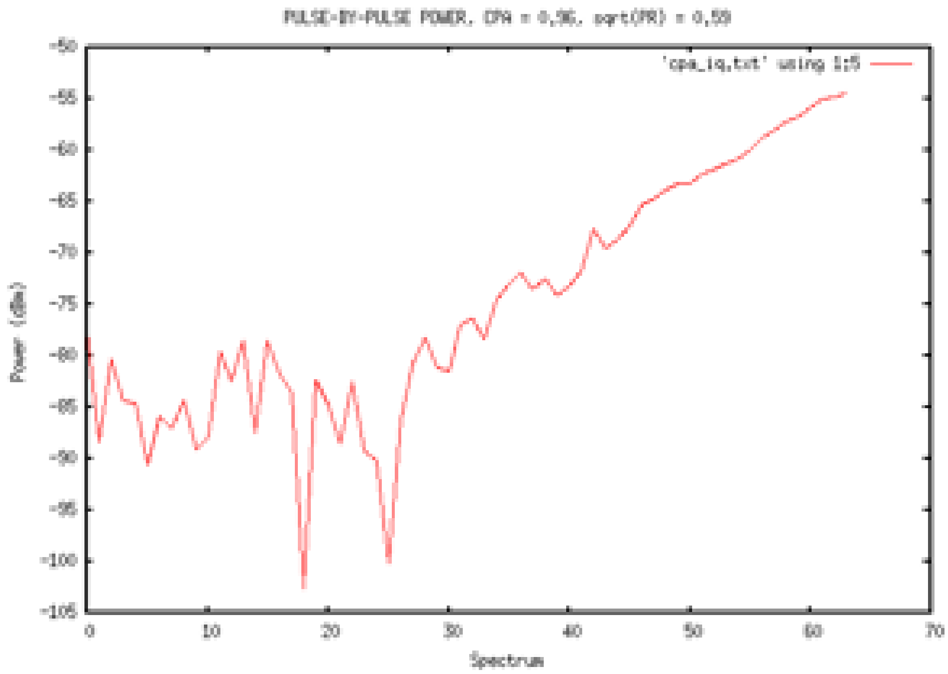


Figure 5: *Time series of* $I^2 + Q^2$ *(dB) for a resolution volume with a clutter target*

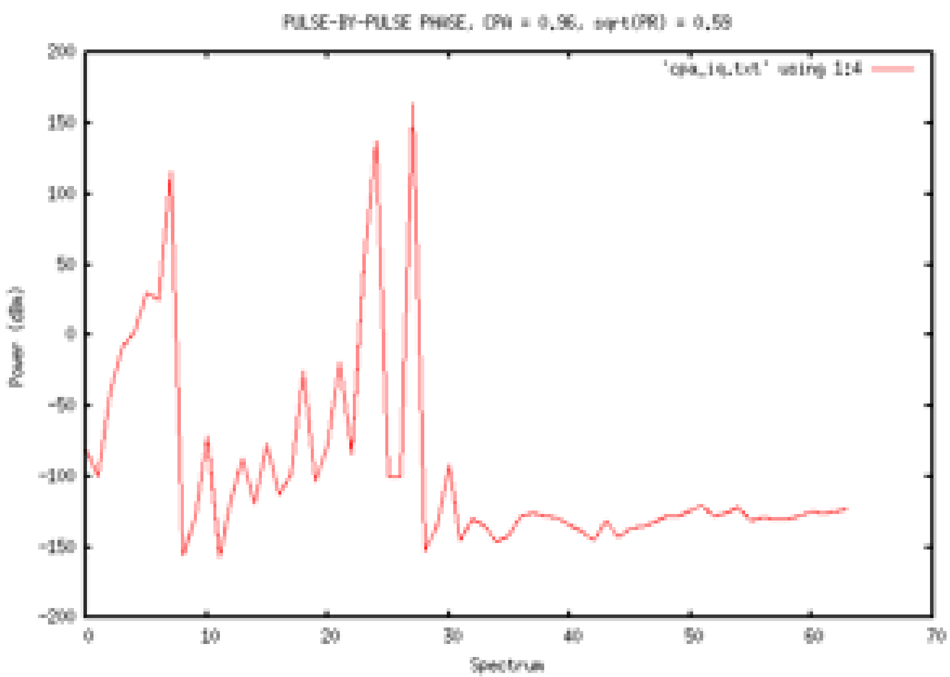


Figure 6: *Time series of* $\tan^{-1}(Q/I)$ *(phase of I and Q) for a resolution volume with a clutter target corresponding to Fig. 5.*

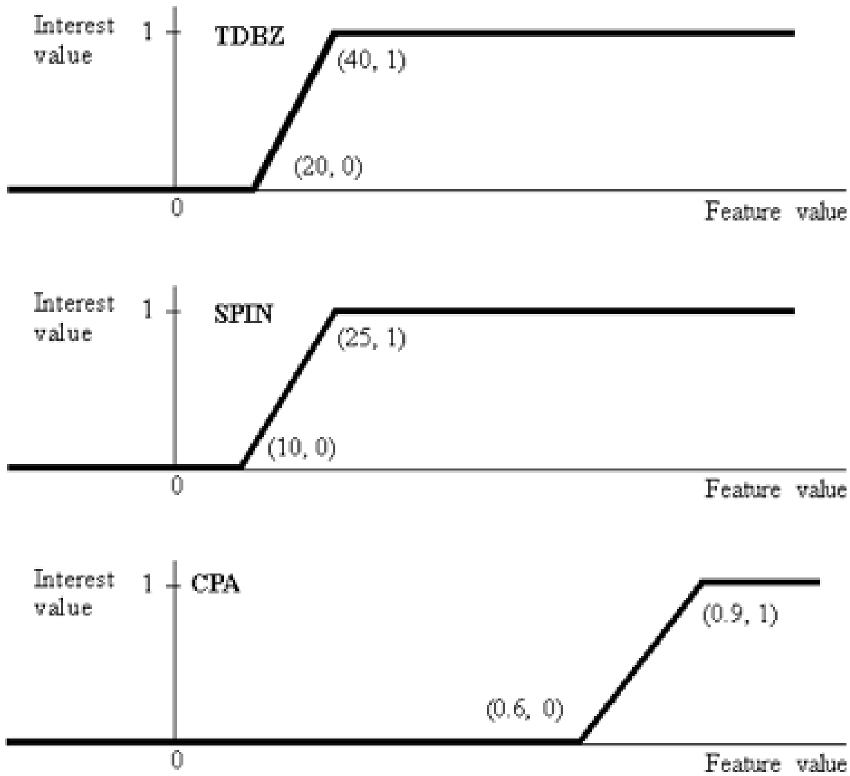


Figure 7: CMD single polarization membership functions.

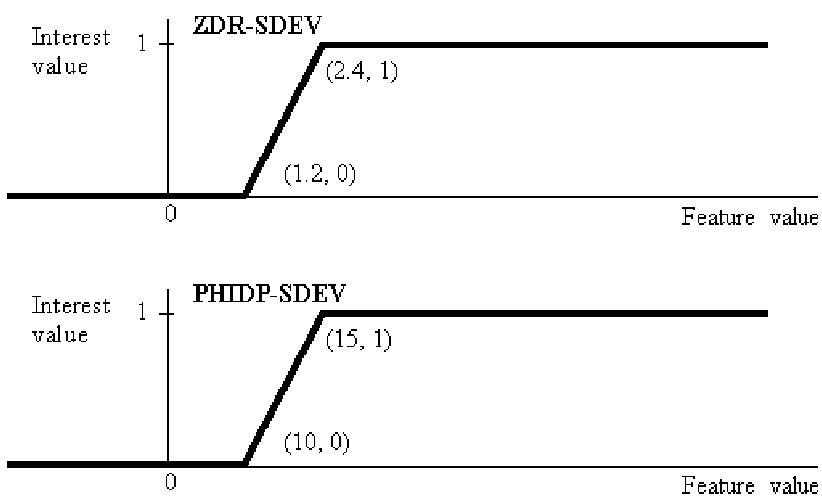


Figure 8: CMD dual polarization membership functions.

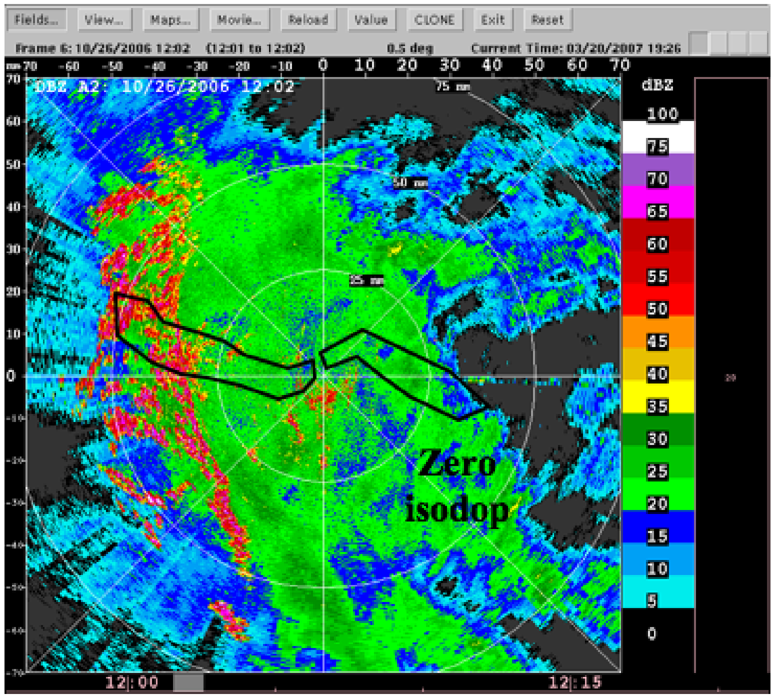


Figure 9: KFTG Unfiltered reflectivity.

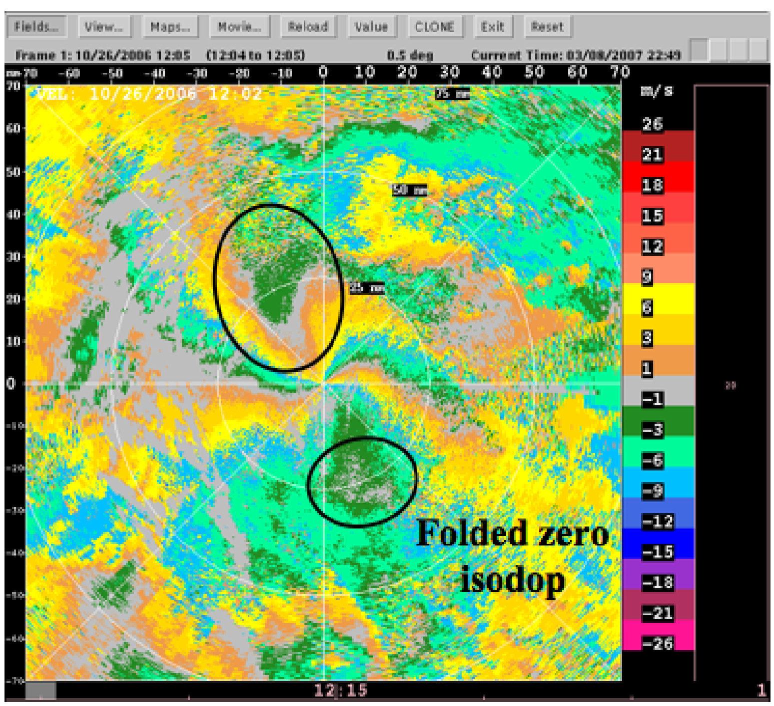


Figure 10: KFTG Unfiltered velocity.

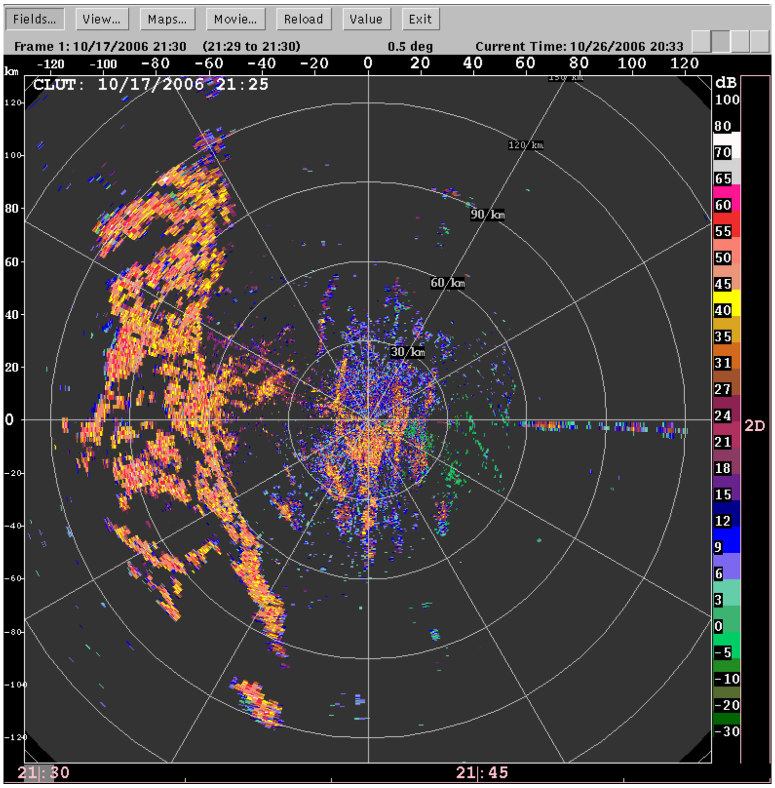


Figure 11: PPI clutter map for KFTG.

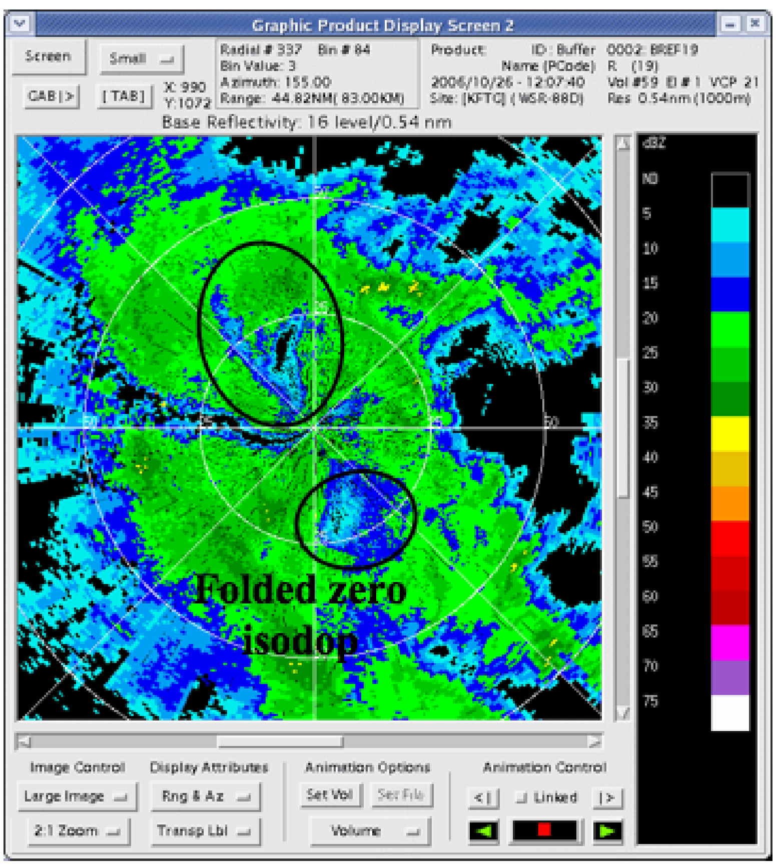


Figure 12: Reflectivity filtered everywhere for data of Fig. 9.

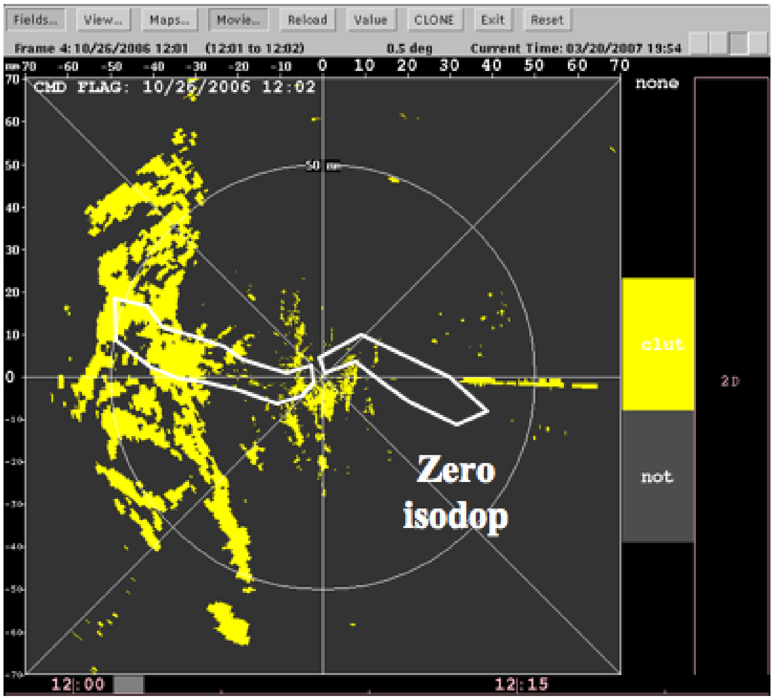


Figure 13: The CMD flag for the KFTG data, i.e., the clutter filter is applied at those gates in the yellow regions.

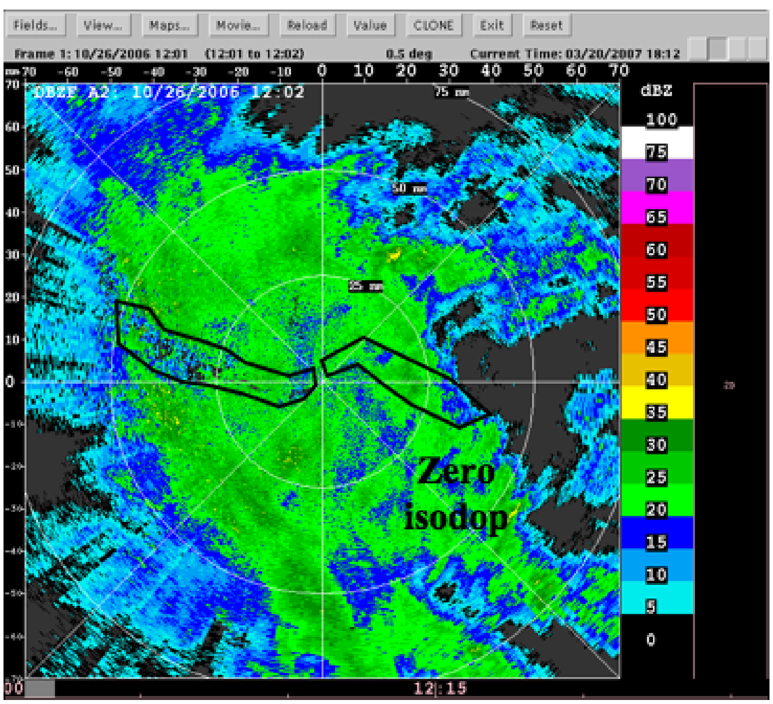


Figure 14: CMD filtered dBZ for data of Fig. 9.

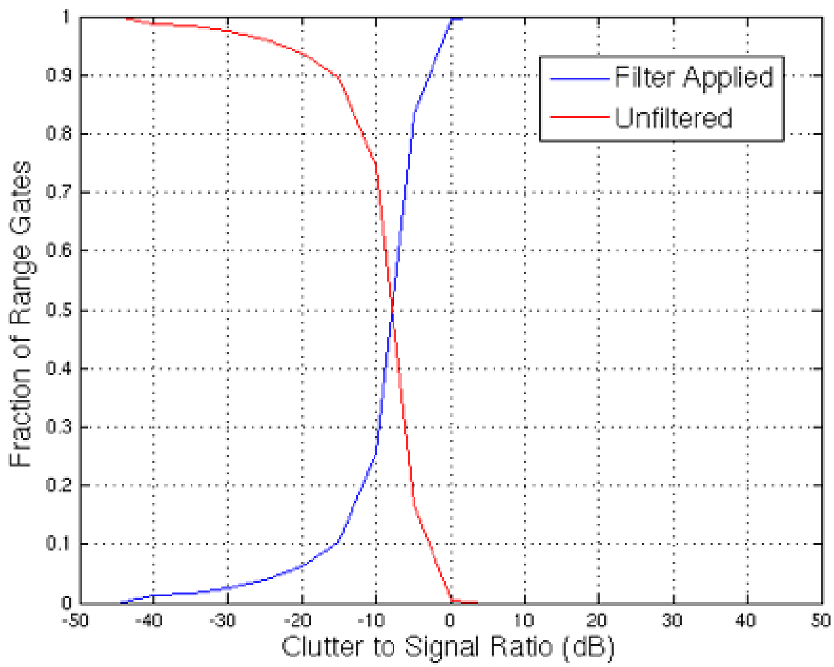


Figure 15: CMD performance.

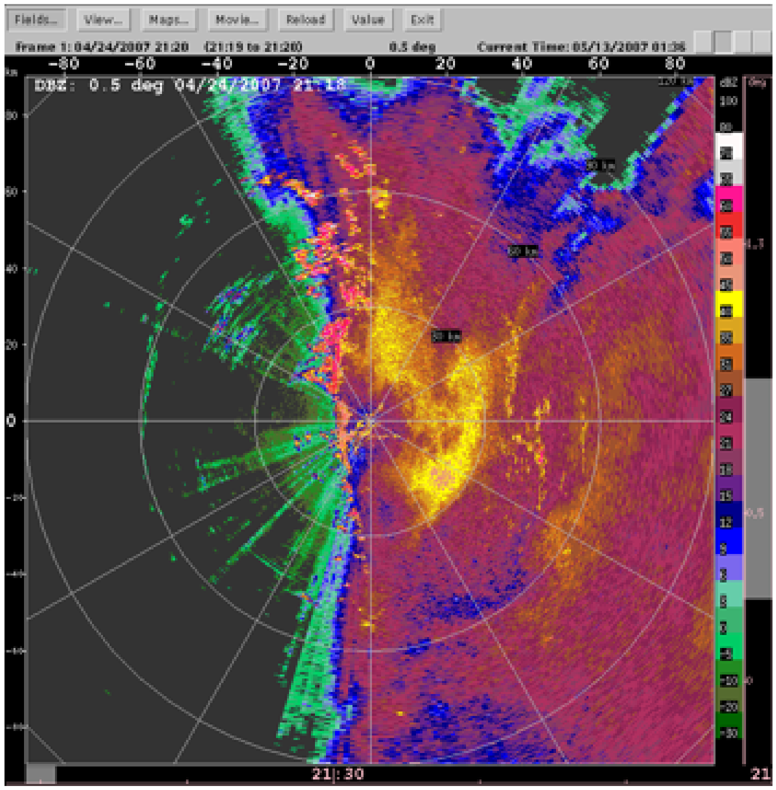


Figure 16: Dual polarization S-Pol case, unfiltered reflectivity.

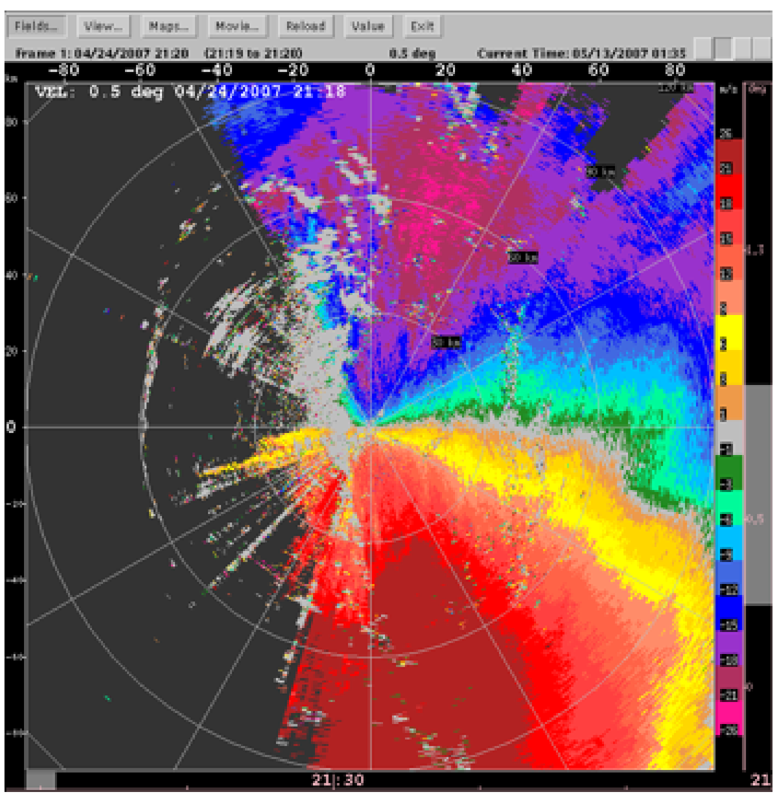


Figure 17: Dual polarization S-Pol case, unfiltered velocity.

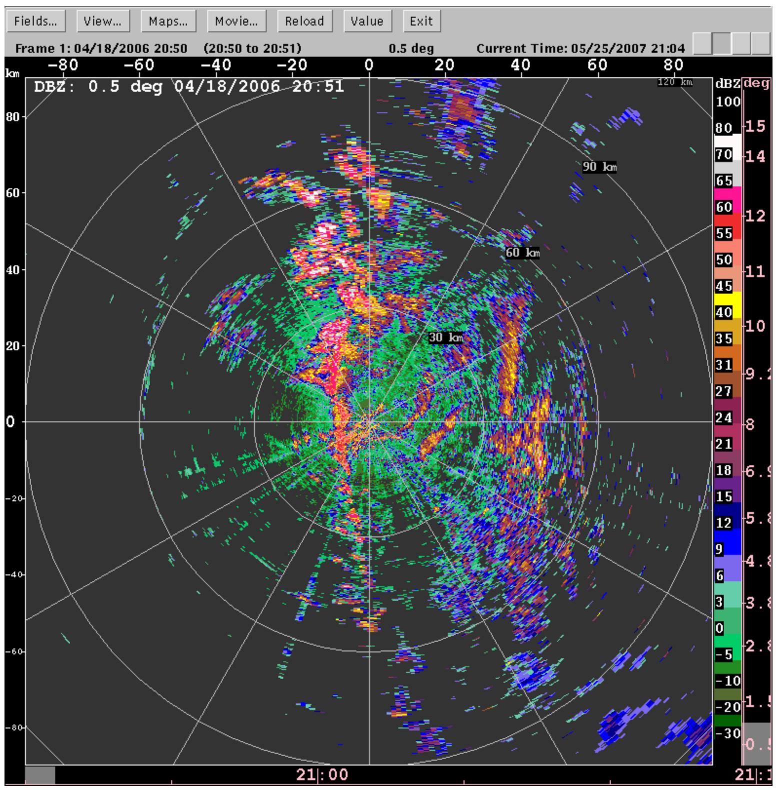


Figure 18: S-Pol Clear air reflectivity.

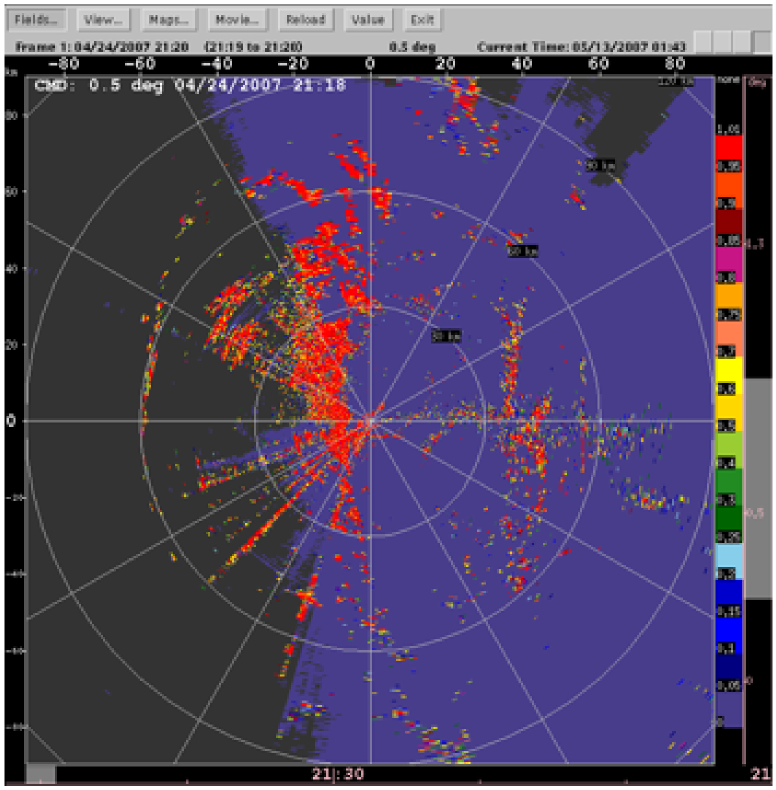


Figure 19: Dual polarization case, CPA interest field.

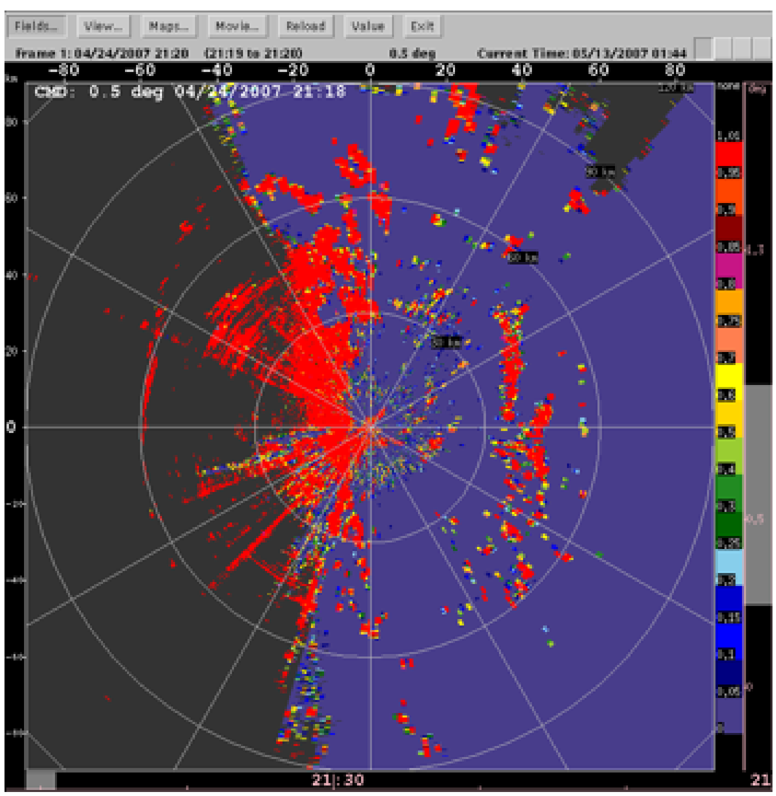


Figure 20: Dual polarization case, standard deviation of $Z_{dr}$ interest field.

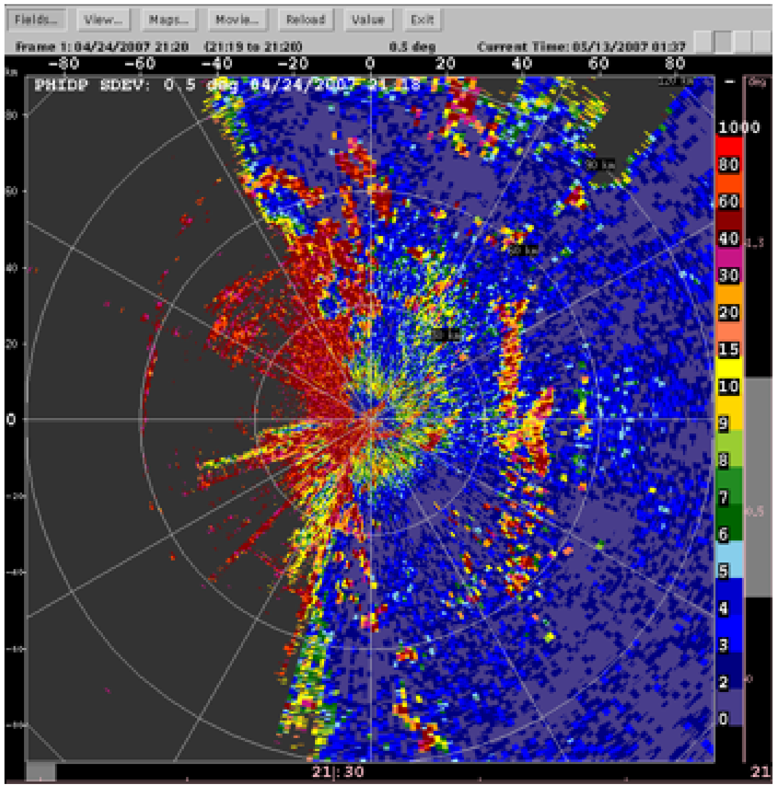


Figure 21: Dual polarization case, standard deviation of $\phi_{dp}$ interest field.

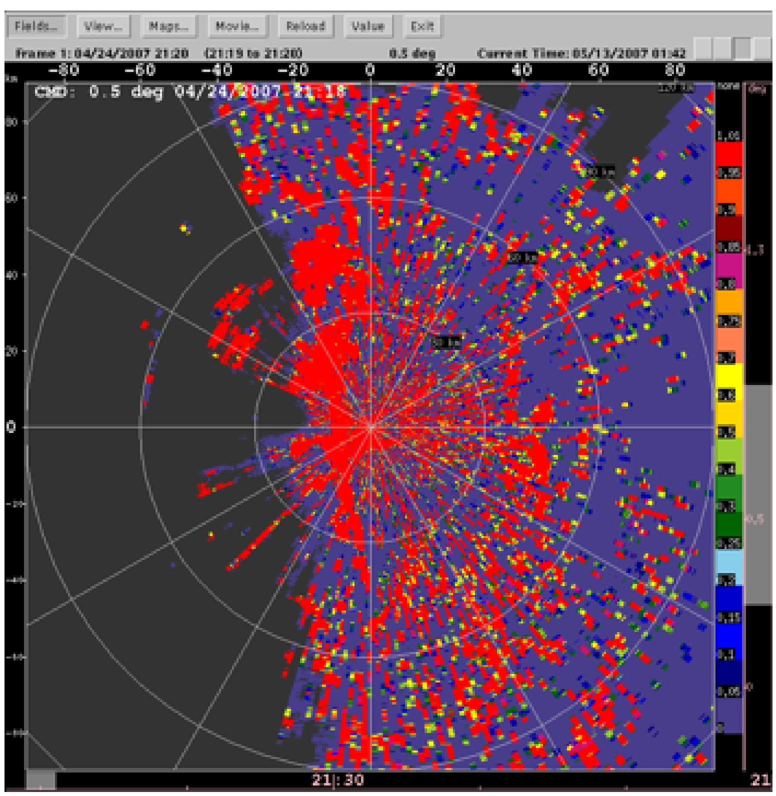


Figure 22: Dual pol. case, TDBZ and SPIN combined interest field.

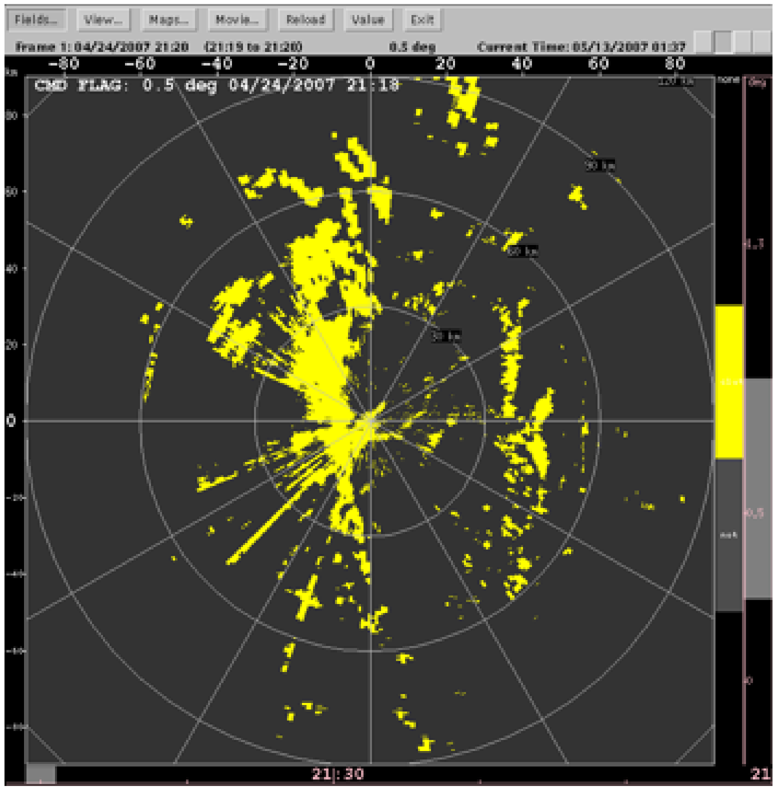


Figure 23: CMD dual pol. clutter flag.

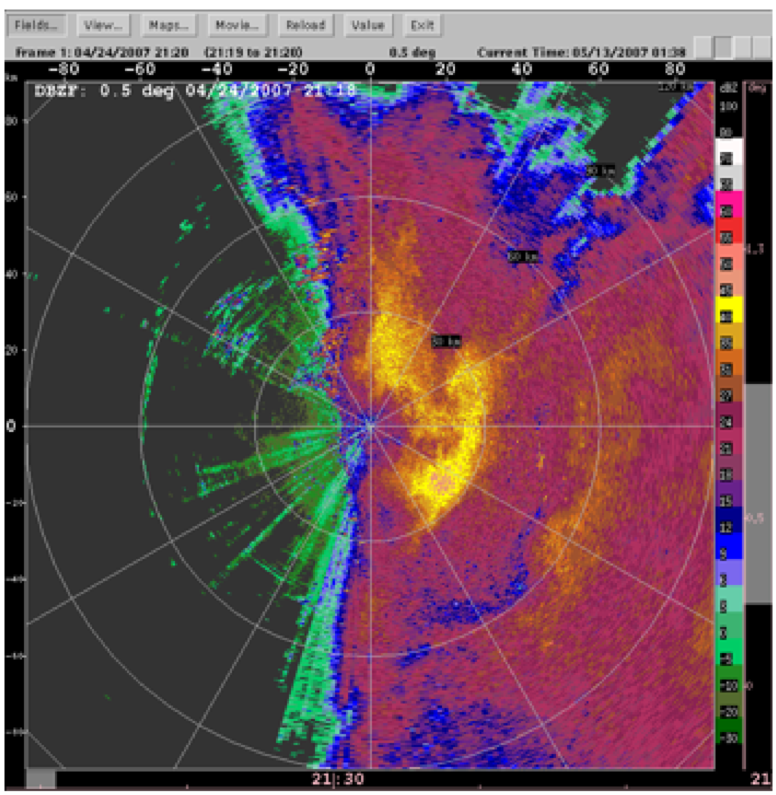


Figure 24: Dual pol. reflectivity filtered. Compare to Fig. 16.